Monitoring mitochondrial biogenesis as the early event for prediction of radiation-induced apoptosis

Chang-Sheng Shao [1,2] , Xiu-Hong Zhou [3] , Yu-Hui Miao [4], Qian-Qian Zhang [1,2] and Qing Huang [1,2] *

[1] CAS Key Laboratory of High Magnetic Field and Ion Beam Physical Biology, Hefei Institutes of Physical Science, Chinese Academy of Sciences (CAS), Hefei 230031, China;

[2] Science Island Branch of Graduate School, University of Science and Technology of China, Hefei 230026, China;

[3] Center of Biology, Anhui Agricultural University, Hefei, China;

[4] Department of Medical Oncology, The First Affiliated Hospital of USTC, Division of Life Sciences and Medicine, University of Science and Technology of China, Hefei, China;

***Corresponding author:**

Prof. Qing Huang

Hefei Institutes of Physical Science, Chinese Academy of Sciences, P. O. Box 1138, Hefei 230031, P.R. China

Tel: 86-551-65595261; Fax: 86-551-65595261

E-mail: huangq@ipp.ac.cn

ABSTRACT

Mitochondrial biogenesis is a cell response to external stimuli which is generally believed to be negatively correlated with apoptosis. However, in the process of apoptosis, whether mitochondrial biogenesis occurs in the early period of the apoptotic cells exposed to the external stimuli such as radiation remains unclear. To address this question, we constructed the COX8-EGFP-ACTIN-mCherry HeLa cells with recombinant fluorescent proteins respectively tagged on the nucleus and mitochondria, and monitored the mitochondrial changes in living cells exposed to the gamma-ray radiation. Besides the in situ and real-time detection of mitochondrial fluorescence changes, we also examined the cell viability, nuclear DNA damage, mitochondrial DNA copy number and the expression of transcription genes of mitochondrial biogenesis and apoptosis marker proteins. As such, we confirmed that mitochondrial biogenesis is taking place preceding apoptosis, and enhancement of mitochondrial biogenesis at at early time is actually positively correlated with the apoptotic cells at late stage.

Keywords: mitochondrial biogenesis; apoptosis; fluorescent proteins; ionizing radiation; living cells; early events

Abbreviations: ANOVA, Analysis of Variance; CCK-8, Cell Counting Kit-8; CytoC, Cytochrome C; DMEM, Dulbecco's modified Eagle's medium;; *E. coli, Escherichia coli*; HCS, High-content screening; H2DCFDA, 2',7'-dichlorodihydrofluorescein diacetate; LDH, Lactate Dehydrogenase; MMP, Mitochondrial membrane potential; MFI, mean fluorescence intensity; Mfn1, Mitofusin 1; mtDNA, Mitochondrial DNA;

44 nDNA, nuclear DNA; PI, Propidium iodide; PARP, Poly ADP-Ribose Polymerase;

45 PGC-1α, Peroxisome proliferator-activated receptor-gamma coactivator (PGC)-1alpha;

46 RT-qPCR, Real-Time Quantitative Reverse Transcription PCR; ROS, reactive oxygen

47 species; SD, standard derivation; TMRE, Tetramethylrhodamine ethyl ester; TFAM,

48 transcription factor A, mitochondrial.

49

Introduction

Mitochondrial biogenesis is a physiological response of cells to external stress and development signals which cause increased energy demand, and it plays an important role in cell metabolism regulation, signal transduction and mitochondrial ROS regulation (Luo et al., 2016; Vyas et al., 2016). Mitochondrial biogenesis maintains cell homeostasis by ensuring the quality of mtDNA and regulating the renewal of organelles(Yambire et al., 2019), and it has been extensively explored in recent years due to its related interests in human aging, neurodegenerative diseases, cell metabolic diseases and tumors(Fanibunda et al., 2019).

Since mitochondrial regulation plays a very critical role in controlling the cell fate, it is intriguing for researchers to explore the relationship between mitochondrial biogenesis and apoptosis. Generally, apoptosis is mediated by the activation of the caspase pathways which are accompanied with mitochondrial damage with destruction of electron transfer, oxidative phosphorylation and ATP production, change of cell redox potential (Burke, 2017). In fact, some studies have claimed that there is a negative correlation between mitochondrial biogenesis and apoptosis, i.e., apoptosis can be suppressed by preceding mitochondrial biogenesis. For example, it has been reported that stress-induced apoptosis can be inhibited by increasing mitochondrial biogenesis (Dam et al., 2013), or, on the other hand, apoptosis and cell cycle arrest can be induced by inhibiting mitochondrial biogenesis (Cao et al., 2017). Also, in the study of radiation-induced apoptosis, mitochondrial biogenesis was observed and analyzed (Rai et al., 2018), and it was claimed that enhancement of mitochondrial biogenesis could reduce the proportion of apoptosis cuased by ionizing

radiation (Yu et al., 2013) . But considering the whole process of apoptosis, whether mitochondrial biogenesis takes place in the early period in the apoptotic cells exposed to the external stimuli such as radiation remains unclear.

To study the process of mitochondrial biogenesis prior to apoptosis, it is crucial to monitor the mitochondrial changes in the cells. At present, there are not many methods available to study the influence of external factors on mitochondrial changes. One of the conventional methods is to detect the change of mitochondrial gene copy numbers (Yu, 2011) . Another approach is to use fluorescent proteins. Fluorescent proteins are beneficial for studying the living cells with reporting gene expression, which can provide information on protein locations and expression levels as well as the involved biochemical activities (Newman et al., 2011) . Actually, study of mitochondria using fluorescent proteins is now emerging (Katajisto et al., 2015; Melentijevic et al., 2017; Ruan et al., 2017). The more recent development is to make use of multiple different fluorescent proteins with different excitation/emission spectra, so that the precision of transcriptional measurements can be ensured by using the reference color for normalization (Miyashiro and Goulian, 2007). In such a circumstance, the ratio of dual fluorescence can be used to eliminate the possible fluorescence measurement errors (Miyashiro and Goulian, 2007) . So with application of this dual fluorescence approach researchers can observe and analyze the temporal and spatial life trajectories of living cells (Jadhav and Shivdasani, 2019) , and maybe more importantly, to scrutinize the early events leading to various bio-effects in the living cells (Yu et al., 2020).

95 Therefore, in the present work, we attempted to apply the dual recombinant
96 fluorescent protein approach to monitor the mitochondrial biogenesis induced by
97 radiation, and in this way, to examine whether and how the early event of
98 mitochondrial biogenesis would be associated with apoptosis. For the effect of
99 radiation as the external stimuli to the cells, it is known that ionizing radiation (such
100 as α-, γ-, X-rays, protons, heavy ions) can easily cause various damages to living cells,
101 which can lead to the change of genetic information, cell mutations, genomic
102 instability, and apoptosis (O'Driscoll and Jeggo, 2006) . Mitochondria, as subcellular
103 organelles, are one of the main targets of ionizing radiation as they occupy a
104 considerable proportion of the cell volume (4-25%) (Leach et al., 2001) . On the other
105 hand, radiation can effectively induce mitochondrial biogenesis (Das et al., 2020) . For
106 the establishment of the dual fluorescent system for in-situ observation of
107 mitochondrial biogenesis in living cells, we constructed the stable fluorescent reporter
108 cell lines by lentiviral transfection to achieve mitoGFP and nuclear RFP, and so we
109 fulfilled the task of real-time in-situ observation of mitochondrial changes in the
110 living cells. As a result, we observed the effect of mitochondrial biogenesis occurring
111 in the early process of the apoptotic cells, and by analyzing fluorescence ratio of
112 mitoGFP and nuclear mCherry fluorescence, we could thus examine the relationship
113 between the early mitochondrial biogenesis and late apoptosis, and so discovered that
114 the increased mitochondria number in the early time was actually positively correlated
115 with the apoptotic cell population. The mitochondrial and apoptotic processes were
116 analyzed and the involved mechanism was discussed.

117 # Results

118 ## Construction of dual-fluorescent stably transfected cell lines

119 In order to construct a universal dual-fluorescence gene reporter vector, we
120 considered to make use of the simplicity of vector construction and referred to the
121 previously reported dual-fluorescence reporter system, and so we chose the CMV
122 promoter to express the dual-fluorescence target proteins. The mitochondrial reporter
123 expression system is generally localized in the stroma, targeting the leader peptide
124 (MSVLTPLLLRGLTGSARRLPVPRAKIHSLGDP) on the VIIIa subunit of
125 cytochrome C (COX8) (Haggie and Verkman, 2002)(Figure 1A). As such, we constructed
126 the pLVX-mCherry-actin lentiviral vector (Figure 1B).

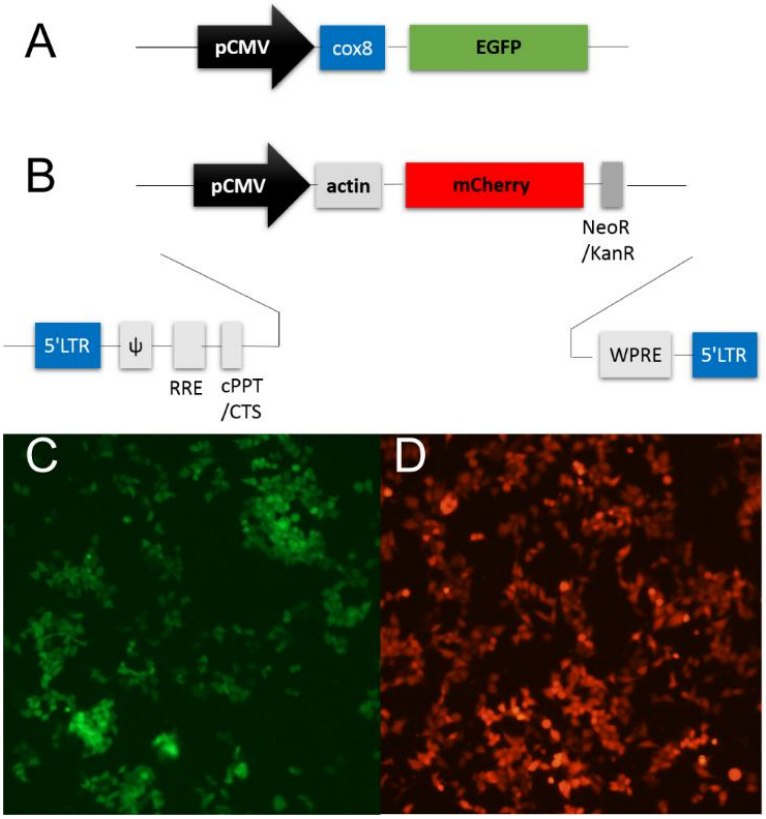

127

128 **Figure 1. Generation of the dual-fluorescent protein reporter system.** (**A**) Schematic
129 illustration of the pEGFP-cox8 reporter system. (**B**) Schematic illustration of the

130 pLVX-actin-mCherry reporter system. (**C**) Fluorescence images of HeLa cells transfected
131 with EGFP-tagged COX8. (**D**) Fluorescence images of HeLa cells transfected with
132 mCherry-tagged Actin.
133
134 To establish the cell line stably co-expressing COX8-EGFP and ACTIN-mCherry,
135 we transfected the HeLa cells with the plasmid containing the expression sequence of
136 COX8-EGFP, and obtained the COX8-EGFP expression cells. After screening by
137 G418 for 2 weeks, the stably transfected cell line was obtained. The
138 COX8-EGFP-mCherry-ACTIN co-expressing HeLa cell line was further established
139 based on the COX8-EGFP expressing cells with lentiviral transfection system. The
140 co-expressions of COX8-EGFP and mCherry-ACTIN were confirmed as shown by
141 the fluorescence microscope examination (Figure 1C, D).
142
143 **In-situ observation with dual fluorescence reporter system**
144 To corroborate our dual-fluorescence reporter system to detect the biological
145 effect in the irradiated living cells, the laser fluorescence confocal microscope was
146 employed. The COX8-EGFP encoding mitochondria (Green), the ACTIN-mCherry
147 encoding actin (Red), and the DAPI-stained nuclei were observed as shown in Figure
148 2.

149

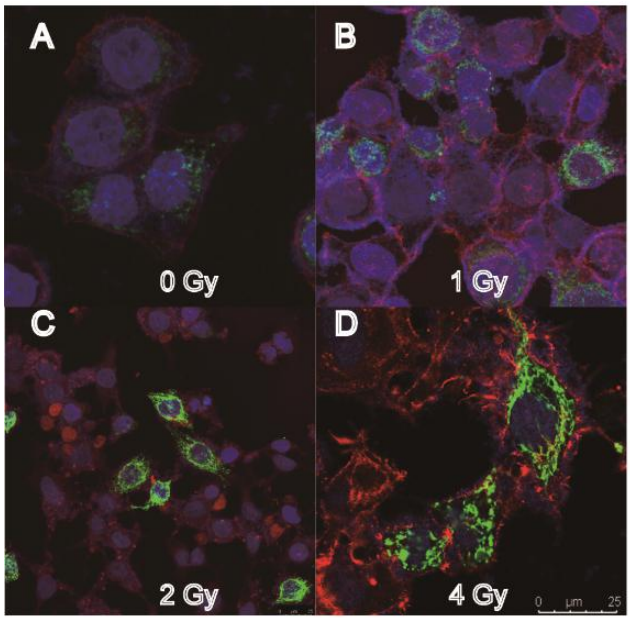

150 **Figure 2. HeLa-COX8-EGFP-ACTIN-mCherry cells exposed to gamma-radiation.** The
151 cells were treated with different doses of γ-ray and observed with confocal laser scanning
152 microscope. In the figure, green color indicates the mitochondria encoding COX8-EGFP, red
153 color shows the actin encoded by actin-mCherry, and blue color represents the DAPI stained
154 nuclei. Scale bar: 25 μm.

155

156 The intracellular mitochondrial content gradually increased as confirmed by laser
157 confocal microscopy visually. Compared with the control group (0 Gy), the irradiated
158 group showed mitochondrial fluorescence enhancement, and it was significantly
159 increased for 2 and 4 Gy irradiation (Figure 2). The fluorescent images intuitively
160 showed that the number of mitochondria increased with increasing radiation dose,
161 confirming that the dual fluorescence reporter system could directly reflect the
162 relevant mitochondrial responses and changes in living cells.

163 **Evaluation of the radiation-induced mitochondrial change using dual-fluorescent**
164 **reporter system**

165 To investigate the mitochondrial fluorescence enhancement of the cells receiving
166 ionizing radiation, the mean fluorescence intensity (MFI) from dual fluorescence
167 reporter system was utilized. Figure 3A shows the numerical changes of two
168 fluorescence channels detected by flow cytometry. The MFI ratio of $EGFP^{+}$:
169 $mCherry^{+}$ was calculated and it was found that the fluorescence ratio was positively
170 correlated with the radiation dose. As shown in Figure 3A, there were significant
171 differences between the irradiated and non-irradiated groups. Besides, this MFI ratio
172 change was observed and recorded in real time by employing High-content Imaging
173 (HCS) system, as shown by Figure 3B. This living cell workstation was employed to
174 record the changes of cell fluorescence within 30 hours after cell irradiation, and the
175 related videos were provided in the Supporting Information (Video 1, 2, 3). The
176 analysis of the fluorescence data indicated that the fluorescence ratio increased
177 significantly with the irradiation dose during the first interval of 1-6 hours, but
178 afterwards, the fluorescence ratio decreased, and the 4 Gy group had a larger
179 declining rate. Lower radiation dose corresponded to the lower rate of reduction of the
180 fluorescence ratio (such as sham group and 1 Gy group). Therefore, the reduction in
181 MFI suggested that the mitochondria of the irradiated cells with higher radiation doses
182 were actually more damaged by the radiation.

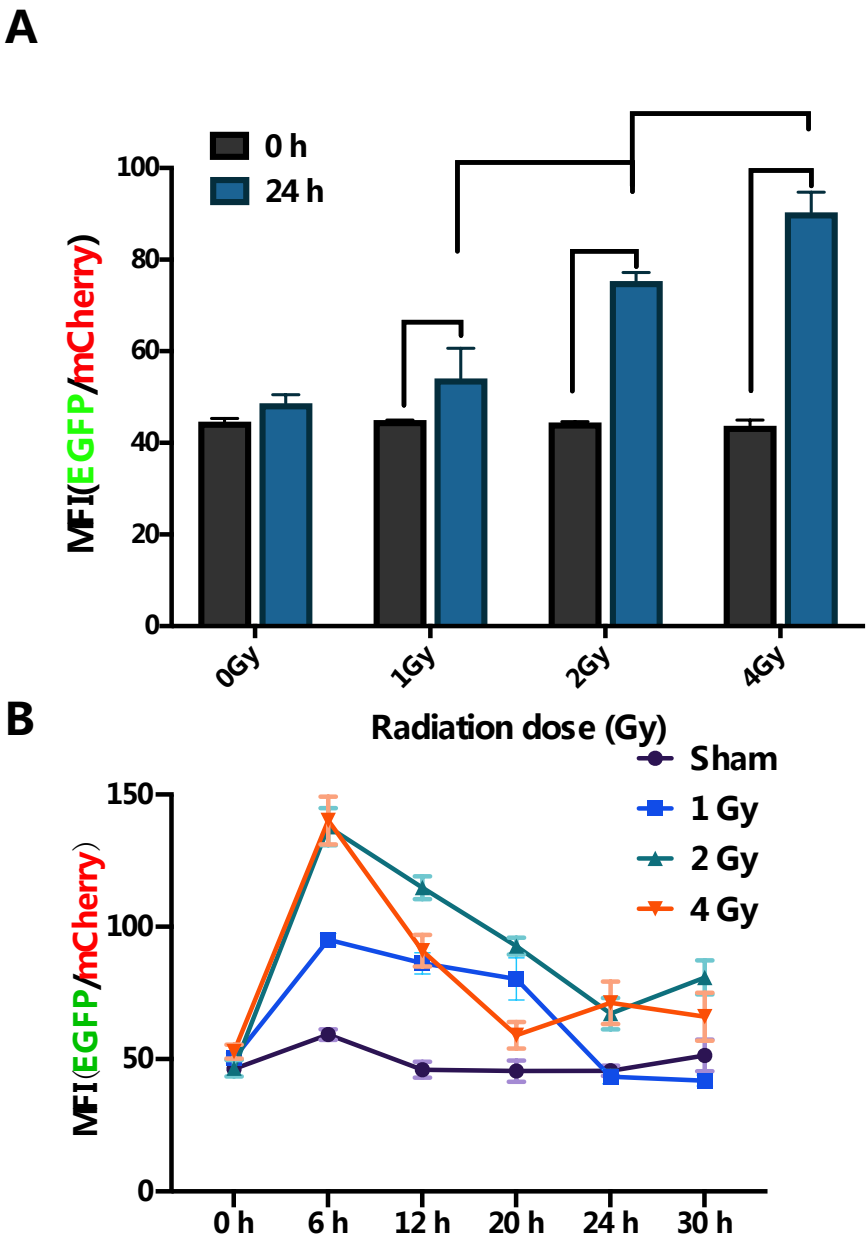

183

184 **Figure 3. The mean fluorescence intensity (MFI) of HeLa cells was determined by flow**
185 **cytometry and High-content Imaging (HCS) Analysis system.**
186 HeLa-cox8-EGFP-actin-mCherry cells were exposed to 1 Gy，2 Gy，4 Gy gamma-ray and
187 incubated for the indicated times. The MFI of HeLa cells by irradiation was determined by
188 flow cytometry and HCS system. Normalized to the average MFI of the positive EGFP cells
189 ratio on the average MFI of the positive mCherry cells. (**A**) The MFI of dual-fluorescent was
190 detected by flow cytometry. (**B**) The MFI of HeLa cells by irradiation was recorded by HCS.

191 **Radiation effects on cell viability, survival rate, cell cycle, apoptosis, DNA**
192 **damage and mitochondrial membrane damage**

193 To investigate the radiation effect, the cell viability was measured by CCK-8
194 method. The results showed that cell viability decreased gradually with the increase of
195 radiation dose (Figure 4A). The toxic effect of radiation on cells was also examined
196 using LDH kit, which revealed that the radiation-induced toxicity was indeed
197 increased significantly with radiation dose (Figure 4B). Also, the colony-forming
198 method was used to analyze the inhibitory effect of γ-ray on HeLa cell survival. With
199 increase of γ-ray irradiation dose, the cell survival rate was only 30% after 4 Gy
200 irradiation (Figure 4C), confirming that the cell survival rate decreased with the rise
201 of radiation dose.

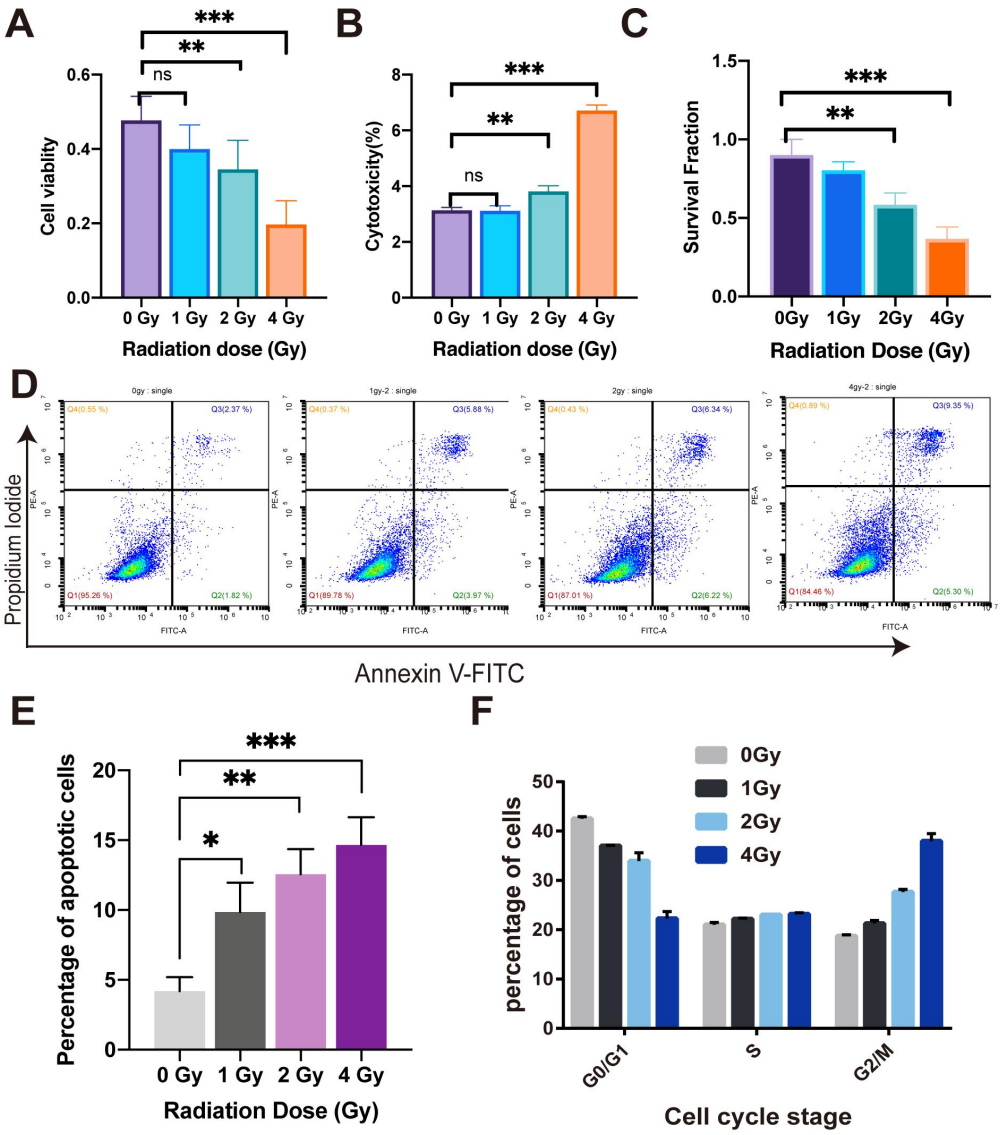

Figure 4. Detection of the radiation effect on HeLa cells with different radiation doses. (**A**) CCK-8 assay for cell viability. (**B**) LDH assay for cell cytotoxicity. (**C**) Colony formation assay of HeLa cells after 14 days under different radiation doses. (**D**) Flow cytometry results of Annexin V-PI assay. (**E**) Apoptotic cells rate. (**F**) Cell cycle examination. The experiment was performed 3 times. Data are presented as Mean±SD; $P<0.01$(**); $P<0.001$(***); ns: not significant compared with untreated cells.

In addition, the cell cycle and apoptosis were assessed for the cells irradiated with γ-ray. Apoptotic cells were detected by flow cytometry after irradiation using Annexin V-PI methods (Figure 4D). Through statistics and comparison of the number of apoptotic cells, the results showed that with the increase of radiation dose, the number

213 of apoptotic cells increased significantly (Figure 4E). Cell cycle was analyzed by flow
214 cytometry. The results showed that all groups of cells had G2 arrest after 24 hours of
215 irradiation, especially at 2 Gy and 4 Gy irradiation doses showed significant G2 arrest
216 (Figure 4F).

217 Furthermore, in order to understand the radiation effects, the radiation induced
218 DNA and mitochondrial membrane damage as well the accompanied ROS change
219 were also examined. For such a purpose, the immunofluorescence method was used to
220 detect DNA damage, H_2DCFDA probe was used to label ROS, and TMRE was used
221 to label mitochondrial membrane potential. Figure 5A showed that with increase of
222 the radiation dose, the foci of the gamma-H2AX increased significantly, and the
223 statistical results showed that the ROS level in the irradiated cells increased with the
224 increase of the radiation dose (Figure 5B- D). At the dose of 2 Gy, the ROS level was
225 the highest, and for the 4 Gy group, there was a significant difference compared with
226 the non-irradiated group. In the meantime, the mitochondrial membrane potential
227 decreased significantly with the increase of radiation dose (Figure 5E, F).

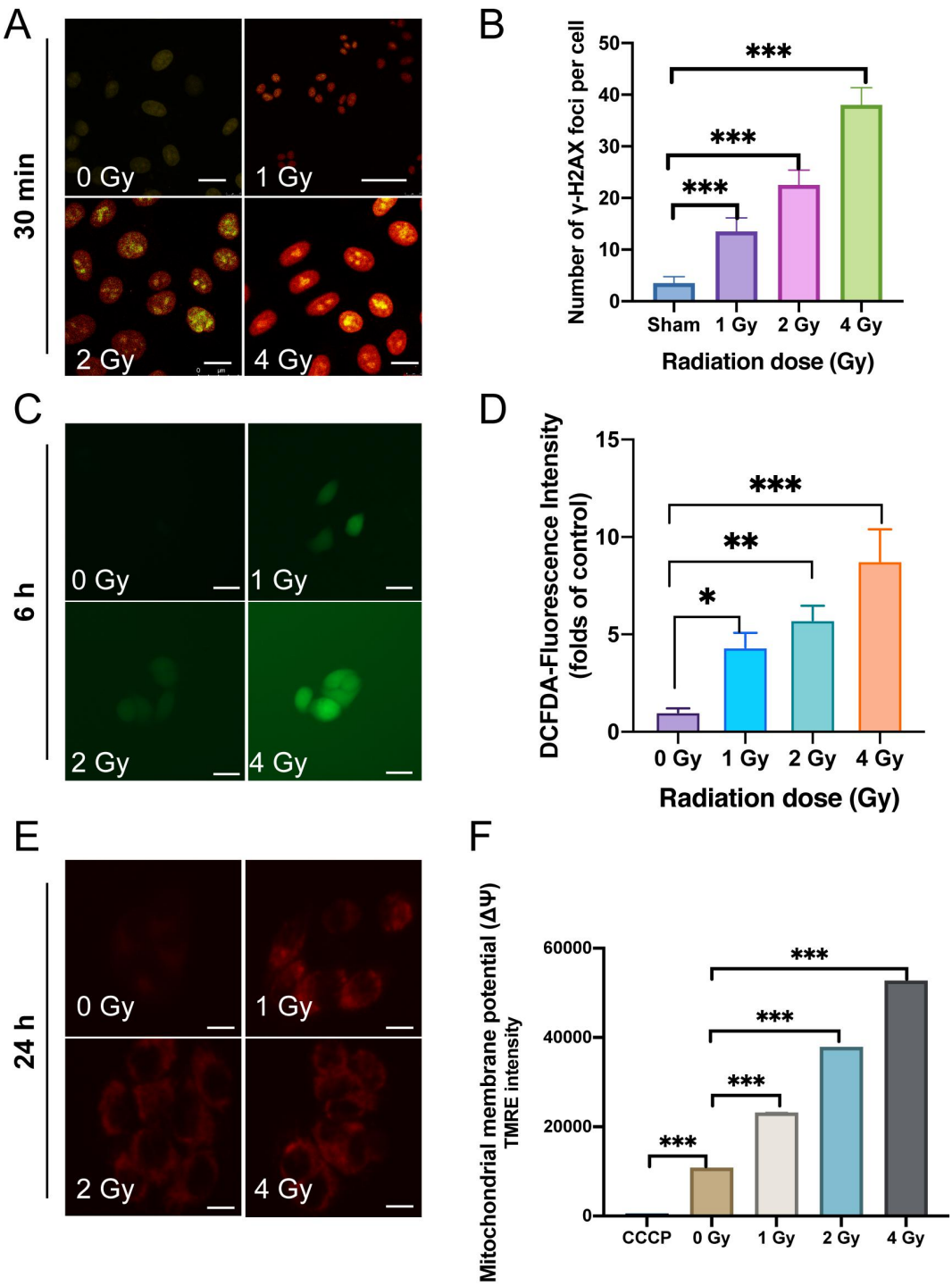

Figure 5. Quantitative analysis of DNA damage level, ROS change level and mitochondrial membrane potential change level after irradiation. (**A**) Representative images of DNA damage detection at different radiation doses when Hela cells were exposed to radiation and measured instantly (within 30 minutes). Green: γ-H2AX; red: DNA stained with PI; Scale bars: 20 μm. (**B**) The graphs show the percentage of populations with the noted number of γ-H2AX foci with different irradiation doses. (**C-D**) ROS assessment using H2DCFDA assay at 6 h. (**E-F**) MMP assay using TMRE at 24 h.

237 **Verification of mitochondrial biogenesis and apoptosis**

238 **Detection of copy number changes of mitochondrial DNA.** To furhter verify the
239 mitochondrial biogenesis induced by radiation, the copy number of mitochondrial
240 DNA was examined. Total DNA was extracted from HeLa cells 6-24 hours after
241 irradiation. As shown in Figure 6, the copy number of mitochondrial DNA also
242 changed after irradiation of the cells. Indeed, under the same radiation dose,
243 mitochondrial DNA number increased with time and compared with the
244 non-irradiated group, and there showed the significant difference. Also, the analysis
245 and comparison of different irradiation groups at the same time point showed that the
246 number of mitochondrial DNA copy increased with radiation dose.

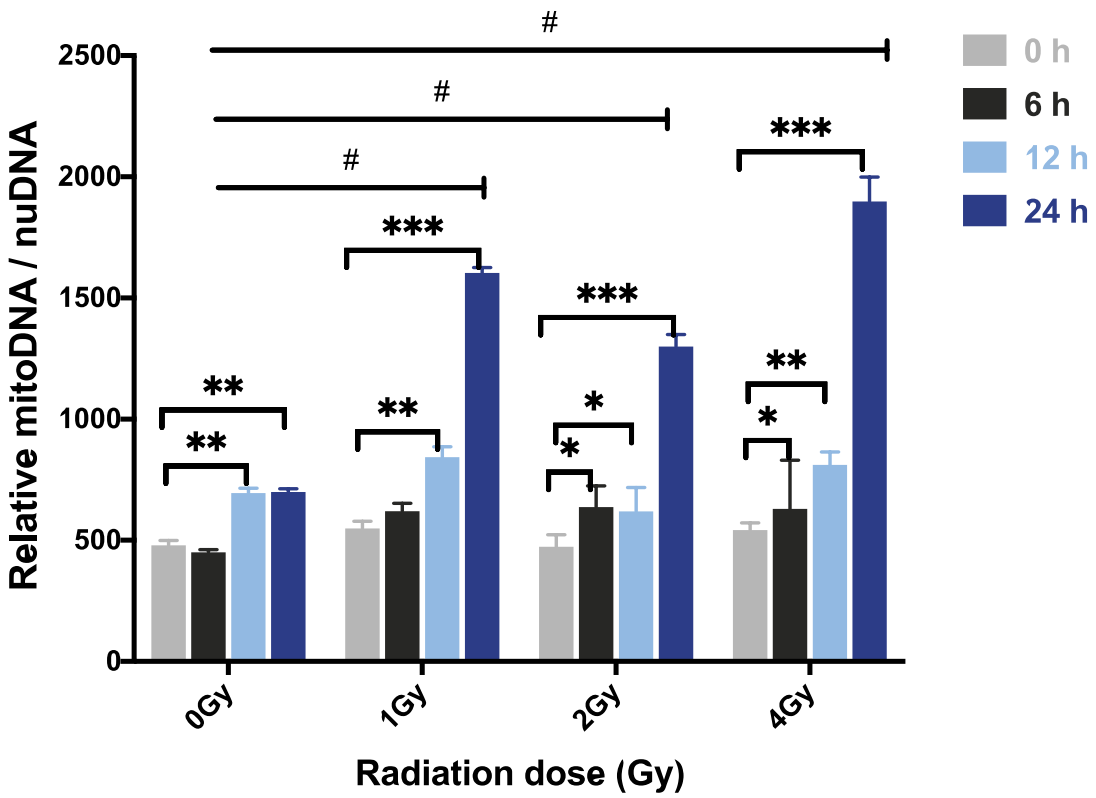

247

248 **Figure 6. Effect of gamma-irradiation on mitochondrial DNA copy number.** HeLa cells
249 were exposed to gamma rays at doses of 1 Gy, 2 Gy and 4 Gy. After 6, 12, 24 hours, total

genomic DNA was extracted and used as a template to detect the mtDNA/nDNA ratio by RT-qPCR. Data are presented as Mean±SD; #: significant compared with unirradiated group; $^{**}P < 0.01$; $^{***}P < 0.001$.

Detection of the related protein expression levels. To explore the correlation between mitochondrial biogenesis and apoptosis under the condition of radiation, the related marker proteins were examined by Western analysis. For the mitochondrial change, the related protein expression levels of PGC-1α, NRF1, TFAM and Mfn1 at different times (6h, 12h, 24h) with different radiation doses (0 Gy, 1 Gy, 2 Gy, 4 Gy) were assessed by Western blot (Figure 7). At 6 hours, the expression level of TFAM protein was increased with radiation dose. On the other hand, for the apoptosis, the related protein expression levels of apoptosis-related marker proteins (BAX, Bcl-2, CytoC, Caspase-3, Cleaved Caspase-9, PARP) were examined. As shown in Figure 7, the expression levels of crucial apoptosis proteins did not differ significantly at early time (6 h), but their expression levels increased significantly afterwards (12 h, 24 h). So these results suggested that there was positive correlation between mitochondrial biogenesis in the early time (6h) and the apoptosis in the late time (24 h).

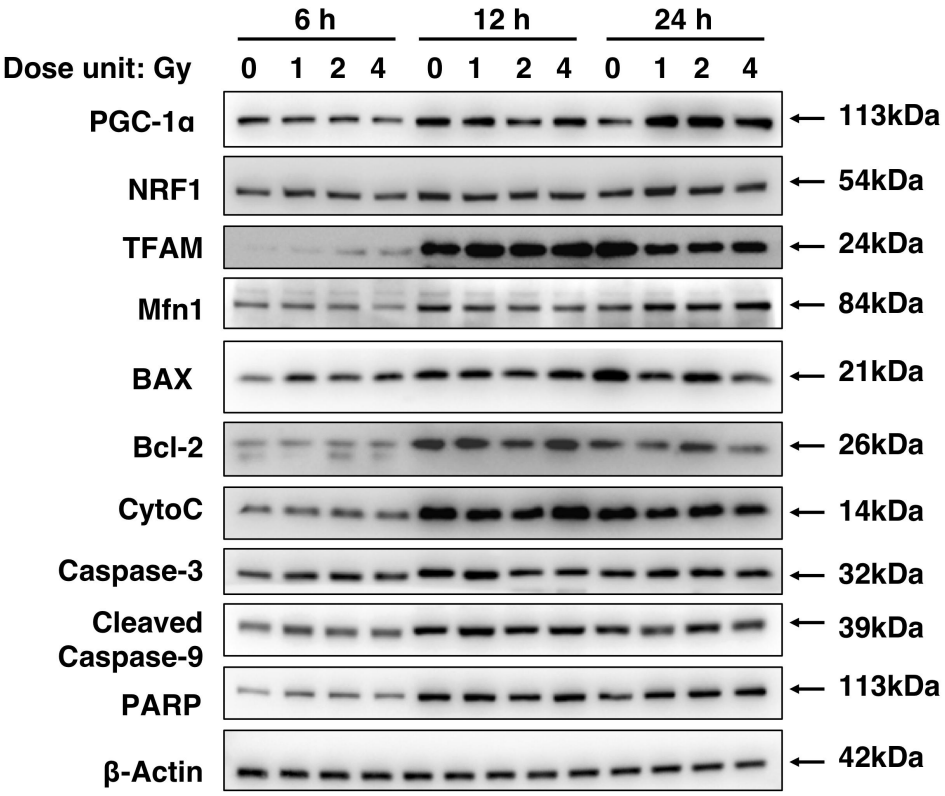

Figure 7. WB assay of the related proteins after radiation treatment. HeLa cells were treated with different doses of irradiation (0, 1, 2, 4 Gy), and total protein was extracted at different time points. Expression level of mitochondrial biogenesis marker proteins (PGC-1α, NRF1, TFAM and Mfn1) and apoptotic marker proteins (BAX, Bcl-2, CytoC, Caspase-3, Cleaved Caspase-9, PARP) by Western blotting.

Discussion

Mitochondria as the cell energy factory play a vital role in cell homeostasis(Lill and Freibert, 2020) In response to external stimuli, mitochondrial biogenesis can be elicited in order to provide the cells with extra energy (Barros and McStay, 2019) . Previously, many studies reported that mitochondrial biogenesis could suppress apoptosis(Yu et al., 2013) i.e., there would be negative correlation between mitochondrial biogenesis and apoptosis. Generally, these studies mainly focused on the cell response to the relatively small stimulus or stress from outside. What would happen if the external

281 stimulus or stress is large enough so that the final fate of apoptosis cannot be avoided?
282 Would mitochondrial biogenesis still go along with the apoptosis in this case? And if
283 it would occur, could we predict the fate of the cells by evaluating the mitochondrial
284 biogenesis as the early event of the cell fate such as apoptosis? With these questions,
285 we thus initiated this research, and applied radiation to induce both mitochondrial
286 biogenesis and apoptosis in the cells, to explore how the mitochondrial biogenesis
287 would be correlated with the apoptosis. As the consequences, we have the following
288 achievements, findings and elaborated understandings.

289 Firstly, we have constructed the dual fluorescence report system that can be
290 effectively used for mitochondrial biogenesis study. To probe the changes taking place
291 in mitochondria, we especially developed the approach using mitochondrial-tagged
292 recombinant fluorescent proteins. The fluorescent protein reporting system has the
293 advantages of real-time, convenient, fast, and non-destructive (Betzig et al., 2006) .
294 Besides, it has also an advantage in the study of subcellular organ localization and
295 protein stress regulation (Llopis et al., 1998) . Previously, people often used fluorescent
296 dye probes for studying effect involved with mitochondria. For example,
297 Mukhopadhyay et al. used Annexin V and Sytox Green and MitoSOX Red fluorescent
298 probes to study the detection of apoptosis and mitochondrial superoxide so as to
299 establish the method for detecting living cells by laser confocal scanning microscopy
300 and flow cytometry (Mukhopadhyay et al., 2007) . But the disadvantages of fluorescent
301 dyes are their toxicity to cells, as well as the light quenching under long-period
302 real-time observation. Compared to fluorescent dyes, fluorescent proteins are stable
303 and have minimal toxicity and can generate visible fluorescence in vivo without the

304 need for external cofactors (Westermann and Neupert, 2000) . Actually, GFP reporter
305 protein is now commonly used to detect mitochondrial changes (Mahajan et al.,
306 1998) (Hanson et al., 2004) . In this work, in particular, we constructed the dual
307 fluorescence reporting system based on fluorescence proteins for the monitoring of
308 mitochondrial changes. This dual fluorescent protein reporter system can not only for
309 the real-time in situ observation for a long time, but also help the precise fluorescence
310 evaluation with the reference fluorescent protein for intensity normalization.
311 Therefore, by analyzing the ratio of the fluorescence intensity of mitochondrial DNA
312 to nuclear DNA expression, the early event of mitochondrial biogenesis under
313 irradiation condition have been readily observed and evaluated, and with this
314 approach we can actually sensitively track the early process which eventually leads to
315 the late event of apoptosis.

316 Secondly, with the as-constructed dual fluorescence report system, we have
317 observed radiation-induced mitochondrial biogenesis preceding the cell apoptosis.
318 Ionizing radiation has been used for cancer therapy for they can directly or indirectly
319 cause DNA damage and kill the cancer cells (Spitz et al., 2004) . With DNA damage in
320 the nucleus, cells may undergo cell cycle arrest required for repairing the damage or
321 cell death including apoptosis (Bernstein et al., 2002) . In parallel, mitochondria is also
322 considered to be the key target for the radiation induced effects, where more reactive
323 oxygen species (ROS) could be produced to cause secondary damage to the cells.
324 Actually, it has been well documented that exposure of cells to ionizing radiation
325 could activate ROS to produce oxidases, regulate antioxidants, and alter metabolic

326 activity in response to oxidative damage (Azzam et al., 2012) . In both the nucleic or
327 mitochondrial processes, more ATP is required to elicit mitochondria biogenesis either
328 directly or indirectly (Kulms et al., 2002; Srinivas et al., 2019) Therefore, mitochondria
329 biogenesis could take place as one of the consequences of radiation-induced
330 bio-effects (Galluzzi and Kroemer, 2008). Interestingly, in our fluorescence measurements,
331 we found that the fluorescence ratio increased and reached the maximum at 6 h after
332 irradiation, but the fluorescence ratio gradually decreased afterwards. So, in the early
333 stage, the fluorescence ratio gradually increased, indicating that mitochondrial
334 biogenesis was enhanced. In this process of mitochondrial biogenesis, mitochondrial
335 DNA and mitochondrial mass are maintained to keep the cell homeostasis and
336 metabolism (Huangyang et al., 2020) . But in the late stage of the radiation effect, the
337 mitochondrial biogenesis gradually decreased. This may be due to the increase of
338 ROS caused by radiation, which continuously increased the oxidative stress that
339 damaged the mtDNA and the mitochondrial integrity. Generally, normal range of ROS
340 may induce stress response by changing the expression of related nuclear genes, and
341 certain level of ROS can save cells by maintaining energy metabolism (Srinivas et al.,
342 2019) . But when the ROS level exceeds the tolerant threshold, ROS can then induce
343 the transition of mitochondrial membrane permeability, leading to the activation of the
344 caspase pathway and promoting cell apoptosis. In our experiment, we indeed detected
345 the increase of ROS level and the decrease of mitochondrial membrane potential. In
346 the meantime, we detected the related caspase related proteins and found that the
347 increase of pro-apoptotic proteins such as cytochrome c. Release of cytochrome c is

348 an indicator for the apoptosis, in which the oxidative stress would damage mtDNA
349 and other components of the cells(Lee and Wei, 2005). Here, we especially noted that the
350 mitochondrial fluorescence intensity decrease rates were quite different after the cell
351 exposure to the radiation. The larger the irradiation dose, the higher the fluorescence
352 ratio reduction rate. This actually confirms the radiation-induced apoptotic process.
353 The mitochondrial damage can be regarded as an early event or signal for
354 apoptosis (Goldstein et al., 2000) As such, the use of dual fluorescence reporter system
355 applied in this work allowed us to observe in situ the cell dynamic process leading to
356 apoptosis, and we could localize fluorescent proteins on the mitochondria in the dual
357 fluorescence reporter system and distinguished the apoptosis process induced by
358 gamma-ray irradiation.

359 Thirdly, our results have revealed the subtle but critical relationship which had
360 not been reported previously. The mitochondrial biogenesis was increasingly
361 associated with the apoptotic stress, and the trend of fluorescence change was
362 consistent with the number of apoptotic cells, and this is actually a new phenomenon
363 contrary to the traditional view on the relationship between mitochondrial biogenesis
364 and apoptosis. In the past, there were few reports regarding the dynamic observation
365 of mitochondrial biogenesis in the early stage. The main reason may be due to lack of
366 in-situ observation method that can deliver the instant and reliable analysis of
367 mitochondrial biogenesis. For example, the traditional methods include using
368 real-time quantitative PCR to detect the copy number of mitochondrial DNA, or using
369 WB to identify the changes of marker protein level of mitochondrial biogenesis.

These methods cannot achieve in-situ and real-time observation in living cells. On the contrary, the fluorescence protein method can be used to observe the mitochondrial biogenesis in real time as especially useful for studying the early events prior to apoptosis. Based on the fluorescence signal, the dual fluorescence ratio can help us to predict the radiation effects or the cell fate according to the fluorescence change of these irradiated cells. For example, from the data obtained from Fig. 3B, the fluorescence ratios can be calculated, and we can retrieve the MFI ratios in each irradiation dose group (0 Gy, 1 Gy, 2 Gy, 4 Gy) at an earlier time (e.g. 6 h), as shown in Figure 8A. Strikingly, this result is consistent with the cells in the apoptotic state at 24 h (Figure 8B). It is understandable because the apoptosis is actually dependent on the early biochemical events in the cells(Holler et al., 2000). In this way, we can therefor infer or predict the late apoptotic state of cells by observing the changes in mitochondrial fluorescence ratio in the early stage.

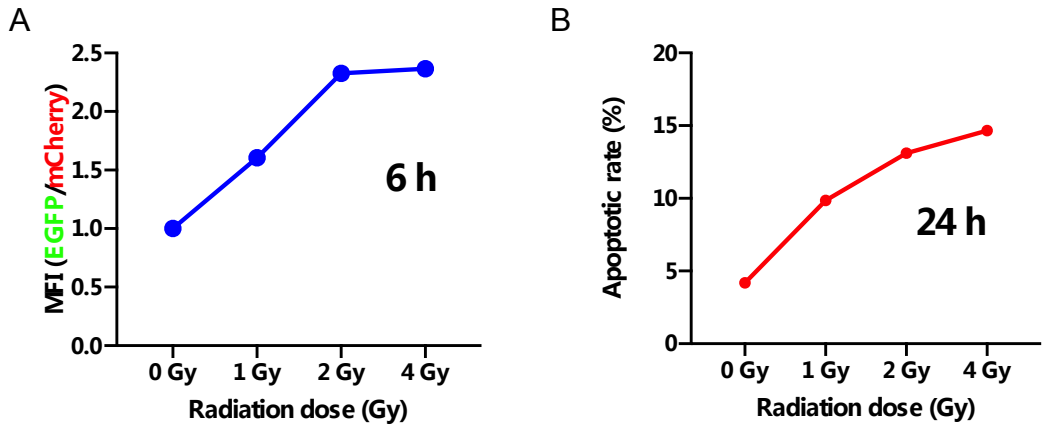

Figure 8. Analysis of mean fluorescence intensity and apoptosis percentage. (**A**) Analysis of EGFP/mCherry ratio in High Content Screening (HCS) at 6h. (**B**) Analysis of apoptotic cells percentage at 24h.

Lastly, we have also tried to understand the mechanism for the mitochondrial

388 biogenesis related to radiation induced apoptosis. For this purpose, we proved that
389 some marker proteins of mitochondrial biogenesis were involved in the biological
390 effects of radiation. We found that the protein and mRNA expression levels of nuclear
391 respiratory factor1 (NRF1), peroxisome proliferative activated receptor, gamma,
392 coactivator 1 alpha (PGC-1α), transcription factor A, mitochondrial (TFAM)
393 increased with increasing irradiation dose. NRF1 is a transcription factor with an vital
394 role in mitochondrial functional genes (Virbasius et al., 1993) PGC-1α is a
395 transcriptional coactivator which is a key inducer of mitochondrial biogenesis (Wu et
396 al., 1999). TFAM is a key activator of mitochondrial (mt) DNA transcription. mtDNA
397 is reported to be very susceptible to oxidative stress(May-Panloup et al., 2005). With the
398 confirmation of these factors, we thus confirmed that this mitochondrial biogenesis is
399 indeed related to radiation induced cell adaptation and apoptosis.

400 So, with the above findings, we can therefore describe the process of radiation
401 affecting cells as depicted in Figure 9. First, after a certain dose of radiation, DNA
402 damage occurs, and the cell cycle is blocked in order to initiate the repair process. At
403 the same time, radiation produces a large amount of ROS in the cell and affects the
404 homeostasis of the cell. To resist the radiation stress or damage, mitochondria then
405 start to provide more ATP for DNA repair and maintenance of cell metabolism and
406 homeostasis, leading to mitochondrial biogenesis. Next, as ROS continues to increase,
407 mitochondrial damage occurs, leading to the decrease in membrane potential, which
408 finally leads to the release of the pro-apoptotic protein cytochrome c, activation of the
409 apoptosis caspase pathway, and so the programmed cell death.

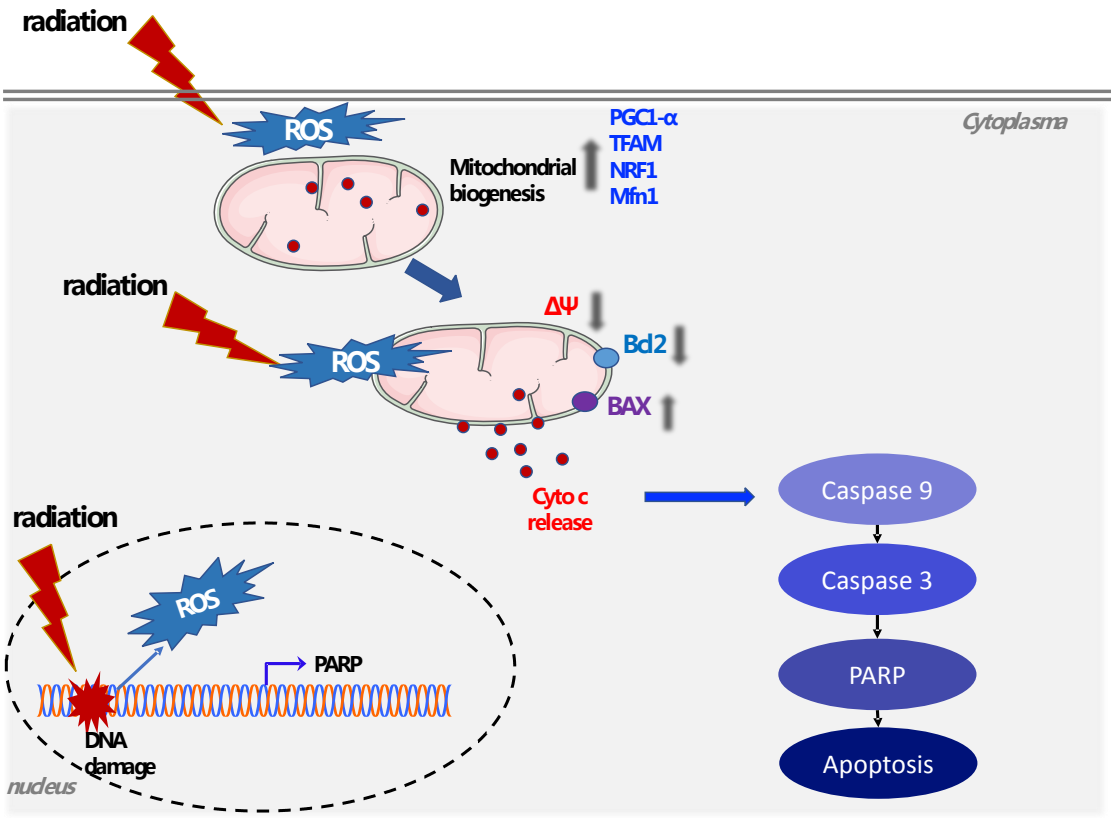

Figure 9. Schematic diagram of biochemical events after ionizing radiation.

SUMMARY

We have constructed a dual fluorescence reporter system, and with the real-time observation and the analysis of the cell fluorescence ratio, we have confirmed the occurrence of mitochondrial biogenesis and apoptosis induced by radiation, and in particular, we have investigated the relationship between this mitochondrial biogenesis and apoptosis, and found there is positive correlation between them with the checkpoint at early stage of cell process which leads to apoptosis. Compared with previous work, this work not only demonstrates how to monitor the mitochondrial biogenesis process but also suggest the way how to predict the radiation-induced biological effects such as apoptosis using the early event observation.

423 # Materials and methods

424 ## Reagents

425 The *Escherichia coli* DH5a and DNA Ladder were purchased from Transgen
426 (Beijing, China). *Nhe*I, *Hind*III, *EcoR*I, *Not*I restriction enzymes, T4 DNA Ligase, and
427 Q5 High-Fidelity DNA Polymerase were purchased from NEB (MA, USA). Plasmid
428 pEGFP-N1 was purchased from Clonetech Biotechnology (CA, USA). Plasmid
429 pLVX-mCherry, PUC57 were stored in our laboratory. Plasmids of psPAX2 (# 12260)
430 and pMD.2G (#12259) were purchased from Addgene. PCR purification and gel
431 extraction kits were obtained from Axygen (CA, USA). TRIzol™ reagent,
432 Lipofectamine 2000 were purchased from Invitrogen (CA, USA). Primescript II 1st
433 strand cDNA Synthesis Kit, RT-qPCR kit and Total genomic DNA extraction kit were
434 purchased from TAKARA (Dalian, China). G418, DAPI was purchased from
435 Beyotime Institute of Biotechnology (Shanghai, China). Reactive oxygen species
436 (ROS) probe 2',7'-dichlorodihydrofluorescein diacetate (H2DCFDA, D6883) was
437 purchased from Sigma-Aldrich. Tetramethylrhodamine ethyl ester (TMRE, T4057)
438 was purchased from Useverbright. The antibodies of PGC-1α, NRF1, TFAM, Mfn1,
439 BAX, Bcl-2, CytoC, Caspase-3, Cleaved Caspase-9, PARP, γH2AX(S139) were
440 purchased from Bimake, anti-β-Actin antibody was purchased from CST(MA, USA).

441 **Creation of stably transfected cell lines**

442 **Generation of plasmids.** Firstly, the pEGFP-N1-COX8 expression plasmid was
443 constructed. Briefly, the DNA sequence of cytochrome c oxidase 8A subunit was
444 found from Genbank (NM_004074.2) (Hendrickson et al., 2010) . Then two
445 complementary oligonucleotide strands were obtained by amplification using PCR,
446 and the restriction sites of the *Nhe*I and *Hind*III were added at both ends. The
447 sequences of oligonucleotide strands were listed in S1 Table. The DNA sequence
448 (COX8A) was ligated on the PUC57 plasmid. Then, the appropriate oligonucleotides
449 were annealed and ligated into pEGFP-N1 cloning cut with *Nhe*I and *Hind*III. After
450 incubation overnight at 37°C, the target plasmids were extracted from the bacterial
451 fluid using the EndoFree Maxi Plasmid kit.

452 Secondly, the PLVX-mCherry-Actin expression plasmid was constructed. Total
453 RNA was extracted from HeLa cells by Trizol reagent and served as the template for
454 cDNA synthesis, and then it was reversely transcripted using Primescript II 1st strand
455 cDNA synthesis kit. The primers were designed according to the sequence of actin
456 (Genbank no. NM_10277): *EcoR*I tailed forward (5′-
457 gtcGAATTCatggatgatgatatcgccgcgc-3′) and *Not*I tailed reverse (5′-
458 TATGCGGCCGCctagaagcatttgcggtggac-3′) primers which are named as
459 Fw-actin-EcoRI and Rv-actin-NotI, respectively. The length of the amplified product
460 was 1128 bp. The PCR product was separated by electrophoresis, and the target
461 fragment was recovered after gel cutting and purification. The target gene fragment

462 (actin) and the expression vector (LVX-mCherry) with the same restriction site
463 (*EcoR*I and *Not*I) were digested by restriction enzymes respectively, and then ligated
464 with T4 ligase and transformed into *E. coli* DH5a for plasmid amplification.

465 **Production of lentiviral supernatant and transduction of**
466 **COX8-EGFP-mCherry-ACTIN-HeLa.** Briefly, positive monoclonal cells
467 (COX8-EGFP-HeLa cells) were constructed. When HeLa cells grew to the
468 concentration of 80% in complete medium, they were then transfected with
469 pEGFP-COX8 plasmid with lipofectamine 2000. After 24-48 h of transfection, G418
470 was added to screen positive monoclonal cells.

471 The lentiviral supernatant was prepared according to the protocol provided by
472 addgene (http://www.addgene.org/tools/protocols/plko/#A). When the confluence of
473 HEK293T cells cells in the 6-well plate reached 80%, Lipofectamine 2000 was used
474 to transfect the pLVX-mCherry-ACTIN plasmid and the viral packaging helper
475 plasmid psPAX2, pMD.2G into the cells. After incubation for 8h, the medium was
476 replaced with the fresh medium containing serum, and the supernatant was collected
477 24 hours and 48 hours later. The virus supernatant was filtered through a 0.45 μm
478 pore so as to infect COX8-EGFP-HeLa cells. Next, the COX8-EGFP-HeLa cells were
479 cultured in a 6-well plate to 70% confluence, then the medium was removed, and the
480 virus supernatant was mixed with fresh medium containing 8 μg/ml polybrene in
481 equal proportions and added to the culture plate. The fresh medium was replaced after
482 24 hours and the medium containing 1 μg/ml puromycin was changed at 48 hours to

483 start screening to obtain stable cell lines.

484 **Cell Culture, Synchronization and Gamma irradiation**

485 HeLa, HEK-293T cell line was purchased from American Type Cultures
486 Collection (ATCC, Manassas, VA). The HeLa and HEK-293T cells were cultured in
487 Dulbecco's modified Eagle's medium (DMEM, HyClone) containing 10% fetal bovine
488 serum (FBS, Gibco BRL). All cells were maintained at 37 °C in 5% CO2.

489 The cell cycle synchronization method was detailed in the previous
490 works (Rodríguez-Martínez et al., 2020) . The cells were incubated with thymidine (2.5
491 mM) for 18 hours, washed once with PBS buffer and replaced with fresh medium for
492 14 hours, and then 2.5 mM thymidine was added again to the cells which were then
493 incubated for 18 hours. The efficiency of synchronization was tested by flow
494 cytometry using cell cycle analysis kit (Multisciences).

495 HeLa cells were gamma-ray irradiated with a Biobeam Cs137 irradiator (cat no.
496 GM 2000; Gamma-Service Medical, Leipzig, Germany) at 1, 2, and 4 Gy witho the
497 dose rate of 3.37 Gy/min. In the control group, the cells were taken out of the
498 incubator without irradiation.

499 **Cell viablity, LDH measurements and colony-formation assays**

500 Cell viability was measured with CCK-8 assay kit (Dojindo, Japan). Briefly, 24 h
501 prior to irradiation treatment, ca. 6000 cells were plated in 96-well plates in a final
502 volume of 100 μl, and then cultured for 24h. And after adding the CCK-8 solution, the
503 plate was incubated for another 1 h. The optical density was measured at 450 nm
504 using a microplate reader (SpectraMax M5, Molecular Devices, USA). The amount of
505 LDH released into the medium was assayed using the LDH-Cytotoxicity Assay Kit II
506 (Dojindo, Japan) according to the manufacturer's instructions. For the colony
507 formation assay, 500 cells were seeded in 6-well plate. After being irradiated, the cells
508 were cultured at 37℃ for about 2 weeks. After carefully washing twice with PBS, 4%
509 paraformaldehyde was added to fix the cells. The the cells were then stained with
510 crystal violet solution and evaluated.

511 **Analysis of mitochondrial membrane potential and ROS**

512 TMRE-Mitochondrial membrane potential (MMP) assay kit (Useverbright, USA)
513 was used to measure MMP. The cells were incubated with culture medium containing
514 200 nM TMRE for 45 minutes at 37 °C, then rinsed with PBS 3 times, followed by
515 incubation with medium containing 50 nM TMRE. For the quantitative assessment,
516 the TMRE staining was evaluated using SpectraMax M5 microplate reader.

517 Reactive oxygen species (ROS) measurement was performed using H2DCFDA
518 (Sigma-Aldrich, USA) probe. 4×10^3 cells were seeded into 96-well plates and
519 incubated overnight. Before irradiation, the cells were incubated with HBSS solution

520 containing 5 μM H2DCFDA for 15 minutes and then irradiated. After 30 minutes, the
521 cells were washed 3 times, followed by the fluorescence measurement using a
522 microtiter plate reader.

523 **Annexin V-FITC/PI staining and cell cycle analysis**

524 The HeLa cells were seeded at 2×10^5 cell /well in 6-well plates and irradiation
525 with gamma-ray. After 24 h, the cells were fixed with cold ethanol and then stained
526 with propidium iodide. The cells (about 20,000) were analyzed by flow cytometry
527 (Beckman CytoFLEX, USA). The total cells were washed once and resuspended in
528 Annexin V binding buffer, and then stained with 5 μl Annexin V and 5μl PI (Roche,
529 Germany) for 20 min and analyzed with Beckman CytoFLEX flow cytometry. Ten
530 thousand events were collected for each sample.

531 **Measurement of mtDNA copy number**

532 Total genomic DNA of HeLa cells was extracted after irradiation using Total
533 genomic DNA extract kit (TAKARA, China). Human nuclear GAPDH gene (forward:
534 5′- CAGAACATCATCCCTGCCTCTAC-3′; reverse: 5′-
535 AAGGGTTGTAGTAGCCCGTAG-3′) and the mtDNA ND1 gene (forward:
536 5′-TTCTAATCGCAATGGCATTCCT-3′; reverse: 5′-
537 AAGGGTTGTAGTAGCCCGTAG-3′), as well as a primer were used to detect the
538 mtDNA copy number. The real-time quantitative PCR analysis was performed using
539 SYBR Premix Ex Taq II (TAKARA, China) on LightCycler 480 PCR System (Roche,

540 Germany). The calculations were analyzed with $2^{-\Delta\Delta Ct}$ method.

541 **Analysis of mean fluorescence intensity（MFI）of dual fluorescent protein**

542 First, MFI of the dual fluorescent protein was analyzed using a flow cytometer.
543 The cells were treated with different radiation doses and collected at different time
544 points, washed once with PBS buffer, then assessed by flow cytometry (Beckman
545 CytoFLEX, USA). The data were analyzed using Flow Jo software. The ratio of the
546 MFI of EGFP to MFI of mecherry was used for calculation and analysis. Each
547 irradiated dose sample group was analyzed for 10,000 cells, and three dishes were
548 repeated.

549 Furthermore, the High-Content Screening system CellInsight CX5 HCS (Thermo
550 Fisher, Waltham, MA) was used for automatic photo quantitative analysis (Sun et al.,
551 2016) . The dual-fluorescent protein HeLa cells were seeded in 96-well plates by
552 irradiated 1 Gy, 2 Gy, 4 Gy gamma ray. The nuclei were stained with Hoechst 33342
553 (Invitrogen, H3570). Fluorescence ratios of protein expression of mitochondrial
554 expressed COX8-EGFP and actin-mCherry were statistically analyzed by cellomics
555 software (Thermo Fisher, Waltham, MA).

556 **Laser scanning confocal fluorescence microscopy**

557 All the images were obtained using 488 nm and 561 nm lasers to excite
558 cox8-EGFP-actin-mCherry, and 405 nm laser lines were used to excite DAPI. The
559 imaging was performed in line mode, the z-stack was over-sampled and photographed

560 at the height of 0.7 microns, and the image was acquired on the LEICA SP8 confocal
561 microscope system. The contrast and brightness of the image were adjusted by
562 Application Suite X (LEICA).

563 **Western blot analysis and immunofluorescence staining**

564 Total proteins were extracted from cells using RIPA lysis buffer with a protease
565 inhibitor cocktail (Roche, Germany). The proteins were quantified using Thermo
566 Scientific Pierce BCA Protein Assay. The protein level of Bax, Bcl-2, caspase-3,
567 cleaved caspase-9, Cytoc, PARP, TFAM, Mfn1, PGC-1α and loading control β-Actin
568 were determined by Western blot assay.

569 For immunofluorescence staining, cells were grown on chamber slides. After
570 gamma-ray irradiation or mock irradiation, they were fixed with cold methanol for 10
571 minutes and permeated with 0.5% Triton X-100 in PBS for 20 minutes. After blocking
572 for 1 hour, the cells were incubated with the primary antibody overnight and then
573 incubated with the fluorescently labeled secondary antibody for 1 hour at 37°C.

574 **Statistical analysis**

575 Data were presented as mean ± standard deviation (SD). Statistical significance
576 was assessed by one-way or two-way ANOVA via GraphPad Prism software (Prism
577 version 8, San Diego, CA, USA). P-Value < 0.05 was considered as statistically
578 significant.

579

Acknowledgments

The authors would like to thank Dr. J. Yan for some preliminary research related to this work. We would also like to thank Drs. Zhiming Zheng and Peng Wang at the Hefei Institutes of Physical Science, Chinese Academy of Sciences for extending their High-content imaging Analysis System facility and providing some consumables for this study. This work was supported by the National Natural Science Foundation of China (grants No. 11635013 and No. 11775272) and Special Repair and Purchase Fund for Central-level scientific institutions (No. Y79XG13361).

Supplementary Information

S1 Table

Oligonucleotides for amplify PCR product of COX8

Oligonucleotides	Sequence 5′ → 3′	size (bp)
Oligo1	CTAGAGATCTGGTACCGTCGACTGCAG AGATCCGCTAGGGGTACTCCGTG CCATCATGTCCGTCCTGACGCCGC TGCTGCTGCGGGGCTTGACAGGC TCGGCCCGGCGGCTCCCAGTGCC GCGCGCCAAGATCCATTCGTTGCC GCCGGAGGGG	154
Oligo2	AGCTTCCCCTCCGGCGGCAACGAATGG ATCTTGGCGCGCGGCACTGGGAG CCGCCGGGCCGAGCCTGTCAAGC CCCGCAGCAGCAGCGGCGTCAG GACGGACATGATGGCACGGAGTA CCCCTAGCGGATCTCTGCAGTCGA CGGTACCAGATCT	155

S1 Video

S2 Video

S3 Video

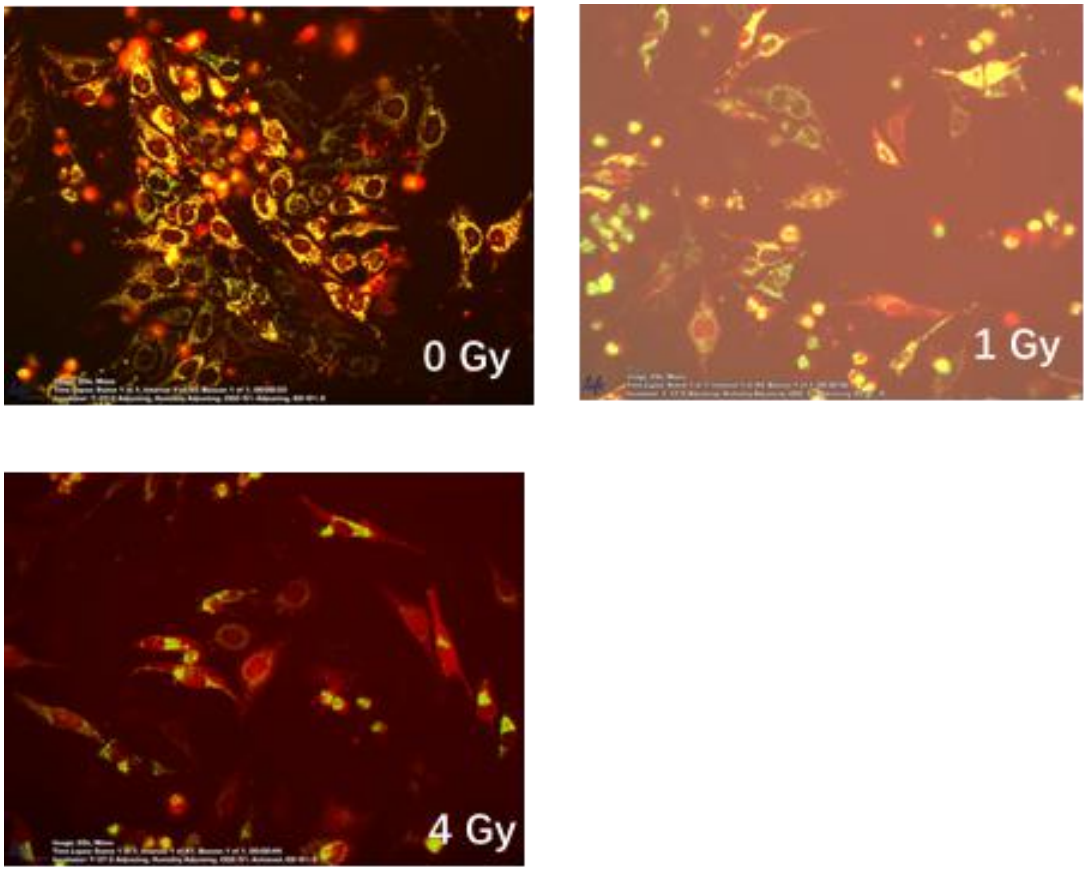

In-situ real-time video of dual fluorescence reporter system of irradiated cells

616 **References:**

617

618 Azzam EI, Jay-Gerin J-P, Pain D. 2012. Ionizing radiation-induced metabolic oxidative stress and
619 prolonged cell injury. *Cancer Lett* **327**:48–60. doi:10.1016/j.canlet.2011.12.012

620 Barros MH, McStay GP. 2019. Modular Biogenesis of Mitochondrial
621 Respiratory Complexes. *Mitochondrion* 50:94－114.
622 doi:10.1016/j.mito.2019.10.008

623 Bernstein C, Bernstein H, Payne CM, Garewal H. 2002. DNA
624 repair/pro-apoptotic dual-role proteins in five major DNA repair
625 pathways: fail-safe protection against carcinogenesis. *Mutat Res Rev*
626 *Mutat Res* 511:145－178. doi:10.1016/s1383-5742(02)00009-1

627 Betzig E, Patterson GH, Sougrat R, Lindwasser OW, Olenych S, Bonifacino
628 JS, Davidson MW, Lippincott-Schwartz J, Hess HF. 2006. Imaging
629 Intracellular Fluorescent Proteins at Nanometer Resolution. *Science*
630 313:1642－1645. doi:10.1126/science.1127344

631 Burke PJ. 2017. Mitochondria, Bioenergetics and Apoptosis in Cancer.
632 *Trends Cancer* 3:857－870. doi:10.1016/j.trecan.2017.10.006

633 Cao C, Yu H, Wu F, Qi H, He J. 2017. Antibiotic anisomycin induces cell
634 cycle arrest and apoptosis through inhibiting mitochondrial biogenesis
635 in osteosarcoma. *J Bioenerg Biomembr* 49:437－443.
636 doi:10.1007/s10863-017-9734-8

637 Dam AD, Mitchell AS, Quadrilatero J. 2013. Induction of mitochondrial
638 biogenesis protects against caspase-dependent and caspase-independent
639 apoptosis in L6 myoblasts. *Biochimica Et Biophysica Acta Bba－Mol Cell*
640 *Res* 1833:3426－3435. doi:10.1016/j.bbamcr.2013.04.014

641 Das S, Joshi MB, Parashiva GK, Rao SBS. 2020. Stimulation of
642 cytoprotective autophagy and components of mitochondrial biogenesis
643 / proteostasis in response to ionizing radiation as a credible
644 pro-survival strategy. *Free Radical Bio Med*.
645 doi:10.1016/j.freeradbiomed.2020.01.015

646 Fanibunda SE, Deb S, Maniyadath B, Tiwari P, Ghai U, Gupta S, Figueiredo
647 D, Weisstaub N, Gingrich JA, Vaidya ADB, Kolthur-Seetharam U, Vaidya
648 VA. 2019. Serotonin regulates mitochondrial biogenesis and function
649 in rodent cortical neurons via the 5-HT2A receptor and SIRT1－PGC-1α
650 axis. *Proc National Acad Sci* 116:201821332.
651 doi:10.1073/pnas.1821332116

652 Galluzzi L, Kroemer G. 2008. Necroptosis: a specialized pathway of
653 programmed necrosis. *Cell* 135:1161–3.
654 doi:10.1016/j.cell.2008.12.004

655 Goldstein JC, Waterhouse NJ, Juin P, Evan GI, Green DR. 2000. The
656 coordinate release of cytochrome c during apoptosis is rapid, complete
657 and kinetically invariant. *Nat Cell Biol* 2:156–162.
658 doi:10.1038/35004029

659 Haggie PM, Verkman AS. 2002. Diffusion of Tricarboxylic Acid Cycle Enzymes
660 in the Mitochondrial Matrixin Vivo: EVIDENCE FOR RESTRICTED MOBILITY
661 OF A MULTIENZYME COMPLEX. *J Biol Chem* 277:40782–40788.
662 doi:10.1074/jbc.m207456200

663 Hanson GT, Aggeler R, Oglesbee D, Cannon M, Capaldi RA, Tsien RY, Remington
664 SJ. 2004. Investigating Mitochondrial Redox Potential with
665 Redox-sensitive Green Fluorescent Protein Indicators. *J Biol Chem*
666 279:13044–13053. doi:10.1074/jbc.m312846200

667 Hendrickson SL, Lautenberger JA, Chinn LW, Malasky M, Sezgin E, Kingsley
668 LA, Goedert JJ, Kirk GD, Gomperts ED, Buchbinder SP, Troyer JL, O'Brien
669 SJ. 2010. Genetic variants in nuclear-encoded mitochondrial genes
670 influence AIDS progression. *Plos One* 5:e12862.
671 doi:10.1371/journal.pone.0012862

672 Holler N, Zaru R, Micheau O, Thome M, Attinger A, Valitutti S, Bodmer J-L,
673 Schneider P, Seed B, Tschopp J. 2000. Fas triggers an alternative,
674 caspase-8–independent cell death pathway using the kinase RIP as
675 effector molecule. *Nat Immunol* 1:489–495. doi:10.1038/82732

676 Huangyang P, Li F, Lee P, Nissim I, Weljie AM, Mancuso A, Li B, Keith B,
677 Yoon SS, Simon MC. 2020. Fructose-1,6-Bisphosphatase 2 Inhibits
678 Sarcoma Progression by Restraining Mitochondrial Biogenesis. *Cell*
679 *Metab* 31:1032. doi:10.1016/j.cmet.2020.04.009

680 Jadhav U, Shivdasani RA. 2019. Dissecting Cell Lineages: From Microscope
681 to Kaleidoscope. *Cell* 176:949–951. doi:10.1016/j.cell.2019.01.054

682 Katajisto P, Döhla J, Chaffer CL, Pentinmikko N, Marjanovic N, Iqbal S,
683 Zoncu R, Chen W, Weinberg RA, Sabatini DM. 2015. Stem cells. Asymmetric
684 apportioning of aged mitochondria between daughter cells is required
685 for stemness. *Sci New York N Y* 348:340–3. doi:10.1126/science.1260384

686 Kulms D, Zeise E, Pöppelmann B, Schwarz T. 2002. DNA damage, death receptor
687 activation and reactive oxygen species contribute to ultraviolet

688 radiation-induced apoptosis in an essential and independent way.
689 *Oncogene* 21:5844–5851. doi:10.1038/sj.onc.1205743

690 Leach JK, Tuyle GV, Lin PS, Schmidt-Ullrich R, Mikkelsen RB. 2001.
691 Ionizing radiation-induced, mitochondria-dependent generation of
692 reactive oxygen/nitrogen. *Cancer Res* 61:3894–901.

693 Lee H-C, Wei Y-H. 2005. Mitochondrial biogenesis and mitochondrial DNA
694 maintenance of mammalian cells under oxidative stress. *Int J Biochem*
695 *Cell Biology* 37:822–834. doi:10.1016/j.biocel.2004.09.010

696 Lill R, Freibert S-A. 2020. Mechanisms of Mitochondrial Iron-Sulfur
697 Protein Biogenesis. *Annu Rev Biochem* 89:471–499.
698 doi:10.1146/annurev-biochem-013118-111540

699 Llopis J, McCaffery JM, Miyawaki A, Farquhar MG, Tsien RY. 1998.
700 Measurement of cytosolic, mitochondrial, and Golgi pH in single living
701 cells with green fluorescent proteins. *Proc National Acad Sci*
702 95:6803–6808. doi:10.1073/pnas.95.12.6803

703 Luo C, Widlund HR, Puigserver P. 2016. PGC-1 Coactivators: Shepherding
704 the Mitochondrial Biogenesis of Tumors. *Trends Cancer* 2:619–631.
705 doi:10.1016/j.trecan.2016.09.006

706 Mahajan NP, Linder K, Berry G, Gordon GW, Heim R, Herman B. 1998. Bcl-2
707 and Bax interactions in mitochondria probed with green fluorescent
708 protein and fluorescence resonance energy transfer. *Nat Biotechnol*
709 16:547–552. doi:10.1038/nbt0698-547

710 May-Panloup P, Vignon X, Chrétien M-F, Heyman Y, Tamassia M, Malthièry
711 Y, Reynier P. 2005. Increase of mitochondrial DNA content and
712 transcripts in early bovine embryogenesis associated with upregulation
713 of mtTFA and NRF1 transcription factors. *Reprod Biol Endocrin* 3:65.
714 doi:10.1186/1477-7827-3-65

715 Melentijevic I, Toth ML, Arnold ML, Guasp RJ, Harinath G, Nguyen KC, Taub
716 D, Parker JA, Neri C, Gabel CV, Hall DH, Driscoll M. 2017. C. elegans
717 neurons jettison protein aggregates and mitochondria under neurotoxic
718 stress. *Nature* 542:367–371. doi:10.1038/nature21362

719 Miyashiro T, Goulian M. 2007. Methods in Enzymology. *Methods Enzymol*
720 423:458–475. doi:10.1016/s0076-6879(07)23022-8

721 Mukhopadhyay P, Rajesh M, Haskó G, Hawkins BJ, Madesh M, Pacher P. 2007.
722 Simultaneous detection of apoptosis and mitochondrial superoxide

723 production in live cells by flow cytometry and confocal microscopy.
724 *Nat Protoc* 2:2295–2301. doi:10.1038/nprot.2007.327

725 Newman RH, Fosbrink MD, Zhang J. 2011. Genetically encodable fluorescent
726 biosensors for tracking signaling dynamics in living cells. *Chem Rev*
727 111:3614–66. doi:10.1021/cr100002u

728 O'Driscoll M, Jeggo PA. 2006. The role of double-strand break repair —
729 insights from human genetics. *Nat Rev Genet* 7:45–54.
730 doi:10.1038/nrg1746

731 Rai Y, Pathak R, Kumari N, Sah DK, Pandey S, Kalra N, Soni R, Dwarakanath
732 BS, Bhatt AN. 2018. Mitochondrial biogenesis and metabolic
733 hyperactivation limits the application of MTT assay in the estimation
734 of radiation induced growth inhibition. *Sci Rep-uk* 8:1531.
735 doi:10.1038/s41598-018-19930-w

736 Rodríguez-Martínez M, Hills SA, Diffley JFX, Svejstrup JQ. 2020.
737 Multiplex Cell Fate Tracking by Flow Cytometry. *Methods Protoc* 3:50.
738 doi:10.3390/mps3030050

739 Ruan L, Zhou C, Jin E, Kucharavy A, Zhang Y, Wen Z, Florens L, Li R. 2017.
740 Cytosolic proteostasis through importing of misfolded proteins into
741 mitochondria. *Nature* 543:443–446. doi:10.1038/nature21695

742 Spitz DR, Azzam EI, Li JJ, Gius D. 2004. Metabolic oxidation/reduction
743 reactions and cellular responses to ionizing radiation: A unifying
744 concept in stress response biology. *Cancer Metast Rev* 23:311–322.
745 doi:10.1023/b:canc.0000031769.14728.bc

746 Srinivas US, Tan BWQ, Vellayappan BA, Jeyasekharan AD. 2019. ROS and the
747 DNA damage response in cancer. *Redox Biol* 25:101084.
748 doi:10.1016/j.redox.2018.101084

749 Sun J, Li N, Oh K-S, Dutta B, Vayttaden SJ, Lin B, Ebert TS, Nardo DD,
750 Davis J, Bagirzadeh R, Lounsbury NW, Pasare C, Latz E, Hornung V, Fraser
751 IDC. 2016. Comprehensive RNAi-based screening of human and mouse TLR
752 pathways identifies species-specific preferences in signaling protein
753 use. *Sci Signal* 9:ra3–ra3. doi:10.1126/scisignal.aab2191

754 Virbasius CA, Virbasius JV, Scarpulla RC. 1993. NRF-1, an activator
755 involved in nuclear-mitochondrial interactions, utilizes a new
756 DNA-binding domain conserved in a family of developmental regulators.
757 *Gene Dev* 7:2431–2445. doi:10.1101/gad.7.12a.2431

Vyas S, Zaganjor E, Haigis MC. 2016. Mitochondria and Cancer. *Cell* 166:555–566. doi:10.1016/j.cell.2016.07.002

Westermann B, Neupert W. 2000. Mitochondria-targeted green fluorescent proteins: convenient tools for the study of organelle biogenesis inSaccharomyces cerevisiae. *Yeast* 16:1421–1427. doi:10.1002/1097-0061(200011)16:15<1421::aid-yea624>3.0.co;2-u

Wu Z, Puigserver P, Andersson U, Zhang C, Adelmant G, Mootha V, Troy A, Cinti S, Lowell B, Scarpulla RC, Spiegelman BM. 1999. Mechanisms Controlling Mitochondrial Biogenesis and Respiration through the Thermogenic Coactivator PGC-1. *Cell* 98:115–124. doi:10.1016/s0092-8674(00)80611-x

Yambire KF, Fernandez-Mosquera L, Steinfeld R, Mühle C, Ikonen E, Milosevic I, Raimundo N. 2019. Mitochondrial biogenesis is transcriptionally repressed in lysosomal lipid storage diseases. *Elife* 8:e39598. doi:10.7554/elife.39598

Yu H, Zhao W, Xie M, Li X, Sun M, He J, Wang L, Yu L. 2020. Real-Time Monitoring of Self-Aggregation of β-Amyloid by a Fluorescent Probe Based on Ruthenium Complex. *Anal Chem* 92:2953–2960. doi:10.1021/acs.analchem.9b03566

Yu J, Wang Q, Chen N, Sun Y, Wang X, Wu L, Chen S, Yuan H, Xu A, Wang J. 2013. Mitochondrial transcription factor A regulated ionizing radiation-induced mitochondrial biogenesis in human lung adenocarcinoma A549 cells. *J Radiat Res* 54:998–1004. doi:10.1093/jrr/rrt046

Yu M. 2011. Generation, function and diagnostic value of mitochondrial DNA copy number alterations in human cancers. *Life Sci* 89:65–71. doi:10.1016/j.lfs.2011.05.010